Electrochimica Acta 56 (2011) 7931–7939

Contents lists available at ScienceDirect

Electrochimica Acta

journal homepage: www.elsevier.com/locate/electacta

Electrodeposition of Zn in acid sulphate solutions: pH effects

Rycharda C.M. Salles [b], Guilherme C.G. de Oliveira [b], Susana L. Díaz [a,1], Oswaldo E. Barcia [a,b,1], Oscar R. Mattos [a,*,1]

[a] LNDC - Laboratório de Ensaios Não-Destrutivos, Corrosão e Soldagem, EE/PEMM/COPPE, Universidade Federal do Rio de Janeiro, UFRJ, Cx. Postal 68505, CEP 21945-970, Rio de Janeiro, RJ, Brazil
[b] Dep. Físico-Química, IQ/UFRJ, Rio de Janeiro, RJ, Brazil

ARTICLE INFO

Article history:
Received 28 July 2010
Received in revised form 6 December 2010
Accepted 8 December 2010
Available online 15 December 2010

Keywords:
Zn electrodeposition
Adsorbed intermediates
Impedance
pH effects

ABSTRACT

The kinetics of zinc electrodeposition from acid sulphate solution on a platinum electrode was investigated by means of stationary polarization curves, interfacial pH measurement and electrochemical impedance spectroscopy. The effect of pH, namely pH 2, 3 and 4, was analyzed. A significant dependence of Zn electrodeposition with solution pH was verified. The results obtained cannot be predicted by the available models for Zn electrodeposition. A reaction model is then proposed based on the predominant steps as a function of the potential and the electrode surface nature.

1. Introduction

Zinc electrodeposition from different media has been the subject of numerous investigations. However, despite the great number of publications on Zn electrodeposition kinetics, this process is still a matter of discussion, since the agreement between the experimental data and the available reaction models is not satisfactory. Different approaches have been associated with a restricted number of experimental results and, for this reason, have not been capable to fully predict the kinetic behaviour of Zn electrodeposition from acid solutions as a function of pH.

In particular, to explain the multiple steady states and the time constants observed in the impedance diagrams obtained during Zn electrodeposition at pH 4.3, not only the adsorbed intermediates interactions [1,2] but also the nucleation and growth processes that give rise to surface relaxation [3,4] have been considered. In the first case, a reaction model proposed by Epelboin et al. [1,2] was based on the competition between the inhibition of adsorbed H^+ and the autocatalytic discharge of Zn^{2+} as well as a reversible adsorption of the anion specific for the electrolyte [1,2]. Later, Zouari and Lapique [5] tried a simplification of this model to describe their results in diluted Zn sulphate solutions. By considering partial dissociation of Zn sulphate, the authors concluded that their stationary results can be grossly fitted by a simple two electron transfer. However, they also recognized that the various physical phenomena involved in the overall Zn deposition from sulphate medium cannot be ignored.

In the other approach, to characterize the electrode kinetics as a function of the morphology of Zn deposits, it was suggested [3,4] that the reactions would occur at specific sites of the electrode surface. Indeed, the inductive feature in the impedance plots was partially ascribed to the slow formation and removal of growth kink sites at the electrode surface, which express the relaxation of the electrode area [3]. However, this consideration fails in simulating the pH effects on the electrodeposition process, especially in what concerns the electrochemical impedance behaviour.

Trying to overcome the limitations on the pH agreement, in later works [6–8] it was suggested that the discharge of Zn^{2+} is inhibited by the hydrogen adsorption in highly acid sulphate solutions. Zn electrodeposition was shown to occur when hydrogen evolution is passivated onto the deposit surface [7]. In this condition, the autocatalytic step in the previous model [1,2] was disregarded, being the strong activation of Zn^{2+} adsorption with increasing polarization the main responsible for progressive Zn deposition predominance. The main restraint to this approach is that it considers a previous free Zn surface. Ichino et al. [8] also introduced modifications on the Epelboin et al.'s [3] model to account for the low frequency capacitive loop observed at low solution pH. However, they considered that this feature is partially ascribed to the diffusion of Zn^{2+} on a

* Corresponding author. Tel.: +55 21 2562 8536; fax: +55 21 2290 1544.
E-mail addresses: susana@metalmat.ufrj.br (S.L. Díaz), omattos@metalmat.ufrj.br (O.R. Mattos).
[1] ISE Member.

0013-4686/$ – see front matter © 2010 Elsevier Ltd. All rights reserved.
doi:10.1016/j.electacta.2010.12.026

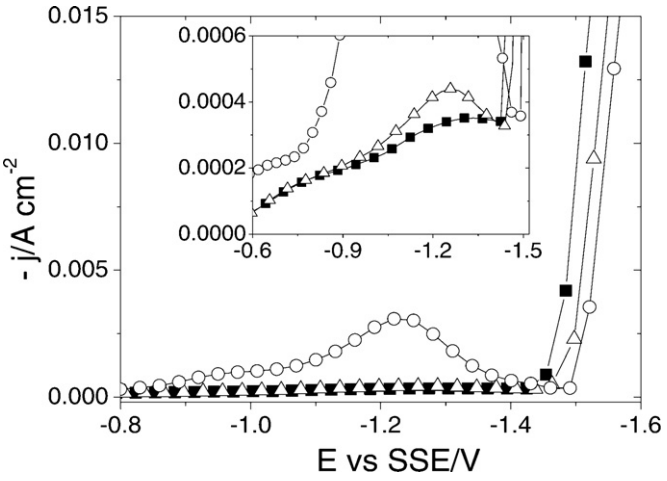

Fig. 1. Steady state cathodic polarization curves of the Pt RDE in the 1 M $ZnSO_4 \cdot 7H_2O$ solution at pH 2 (○), 3 (△) and 4 (■).

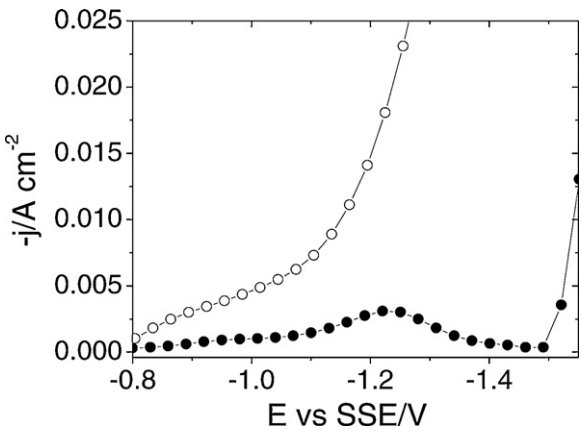

Fig. 2. Steady state cathodic polarization curves of the Pt RDE in both 1 M Na_2SO_4 (Zn^{2+}-free) (○) and 1 M $ZnSO_4 \cdot 7H_2O$ (●) solutions at pH 2.

motionless electrode. Accordingly, the pH effect was not efficiently addressed.

The model proposed for acid sulphate electrolyte [7] was also adapted to describe the Zn deposition mechanism in chloride solution [9], since the deposition mechanism was considered to occur from Zn^{2+}. By using the same reasoning, a simplified model for a fixed solution pH was proposed to account for the charge transfer reactions and the elementary steps of crystal growth.

Although exerting a significant influence on the kinetics of Zn electrodeposition, the role of simultaneous H^+ reduction has gained little attention and is still poorly understood. Since the interfacial pH changes when the hydrogen reduction occurs, the chemical equilibrium of the species present in solution is also modified. It was shown that H^+ reduction is inhibited by the presence of Zn^{2+} ions in solution [7,10,11]. Van Parys et al. [12] considered that, besides the deposition of Zn, ZnO is also formed due to a pH shift during Zn electrodeposition from acid sulphate solution. Although not presenting the corresponding experimental data, the authors stated that a strong increase on the interfacial pH occurs, giving rise to hydroxilated intermediate species. Other works [13–15] also assume the same interfacial alkalination effect to describe the nucleation and growth behaviour during Zn deposition from acid solution.

From the above discussion the elementary steps that take place during Zn electrodeposition were discretized for the proposition of reaction models. However, such models still need experimental validation, particularly with regard to a wide acid pH range. In this sense, the objective of the present work is to systematically investigate Zn electrodeposition from acid sulphate solution in a broad pH range, with special attention to the role of simultaneous H^+ discharge. The goal is to provide a deeper insight into the electrode reaction mechanism, aiming to a more comprehensive model for Zn electrodeposition.

2. Experimental

The electrolyte used in this work consisted of 1.0 M $ZnSO_4 \cdot 7H_2O$ solution at three different pH values: 2, 3, and 4. Sodium sulphate solutions at the same concentration and pH values were also employed as blank solutions (Zn^{+2}-free). The solutions were prepared from analytic grade chemicals and double distilled water, without addition of any other substance such as additives, complex agents or supporting electrolyte. The pH adjustment was done by means of 1.0 M sulphuric acid additions. All experiments were performed in triplicate, at 25 °C and with a large volume of electrolyte (4 l), which was circulated by means of a peristaltic pump. This procedure was carried out to avoid variations on the solution concentration and pH during the electrochemical measurements.

Cathodic potentiostatic polarization curves and electrochemical impedance measurements, in both potentiostatic and galvanostatic modes, were carried out in a conventional three-electrode cell, by means of a model Asservissement Electronique rotating electrode device, using a Pt rotating disc electrode (RDE) with 0.2 cm^2 as working electrode. Some experiments were also performed using a Zn RDE (0.3 cm^2). All tests were accomplished at 1000 rpm of electrode rotation speed to assure the absence of mass transport effects. The counter electrode was a circular Pt grid (300 cm^2) and a saturated mercurous sulphate electrode (SSE) (−0.64 V vs SHE) was used as reference. All the potential values given in this work were always against SSE. The polarization curves were obtained through a model PGSTAT30 AUTOLAB electrochemical interface using the Linear Sweep Polarization Staircase (Stationary Current) method with 30 mV of potential step. A PG19 OMNIMETRA potentiostat and a frequency response analyzer SOLARTRON SI1254 coupled with a PC were used in the impedance measurements. The signals were filtered by a model VBF-8 KEMO Filter in low-pass mode. In most of the experiments, the impedance diagrams were obtained in the frequency interval of 40 kHz to 3 mHz with the amplitude ranging from 5 to 15 mV, within the linearity range. The polarization curves were corrected from ohmic drop through the high frequency part of the electrochemical impedance plots.

For the pH measurements at the electrode/electrolyte interface, a working electrode of the type already proposed was applied [16,17]. It consisted of a 75 mesh Pt grid (3.5 cm^2) held at the end of a flat-bottomed glass electrode (Orion mod. 8135 BN) using of a Teflon adaptor. The pH electrode was connected to a pH meter, thus measuring the pH of the solution retained in the mesh. The assembled electrode was motionless and the solution was stirred to guarantee uniform bulk pH, as detailed elsewhere [10]. Under these conditions, surface pH and current measurements were recorded simultaneously as the electrode was potentiostatically polarized.

3. Results

Fig. 1 presents the cathodic polarization curves obtained with Pt RDE in the 1 M $ZnSO_4 \cdot 7H_2O$ solution in three different pH values: 2, 3, and 4. From these curves, two distinct regions can be observed independently of the pH. In the first one (Part 1), beginning at the open circuit potential, the curves show a slow variation of current with cathodic polarization. In this region, the efficiency for metallic deposition is negligible and the H^+ reduction reaction prevails. With further polarization increase, the current densities show a sudden

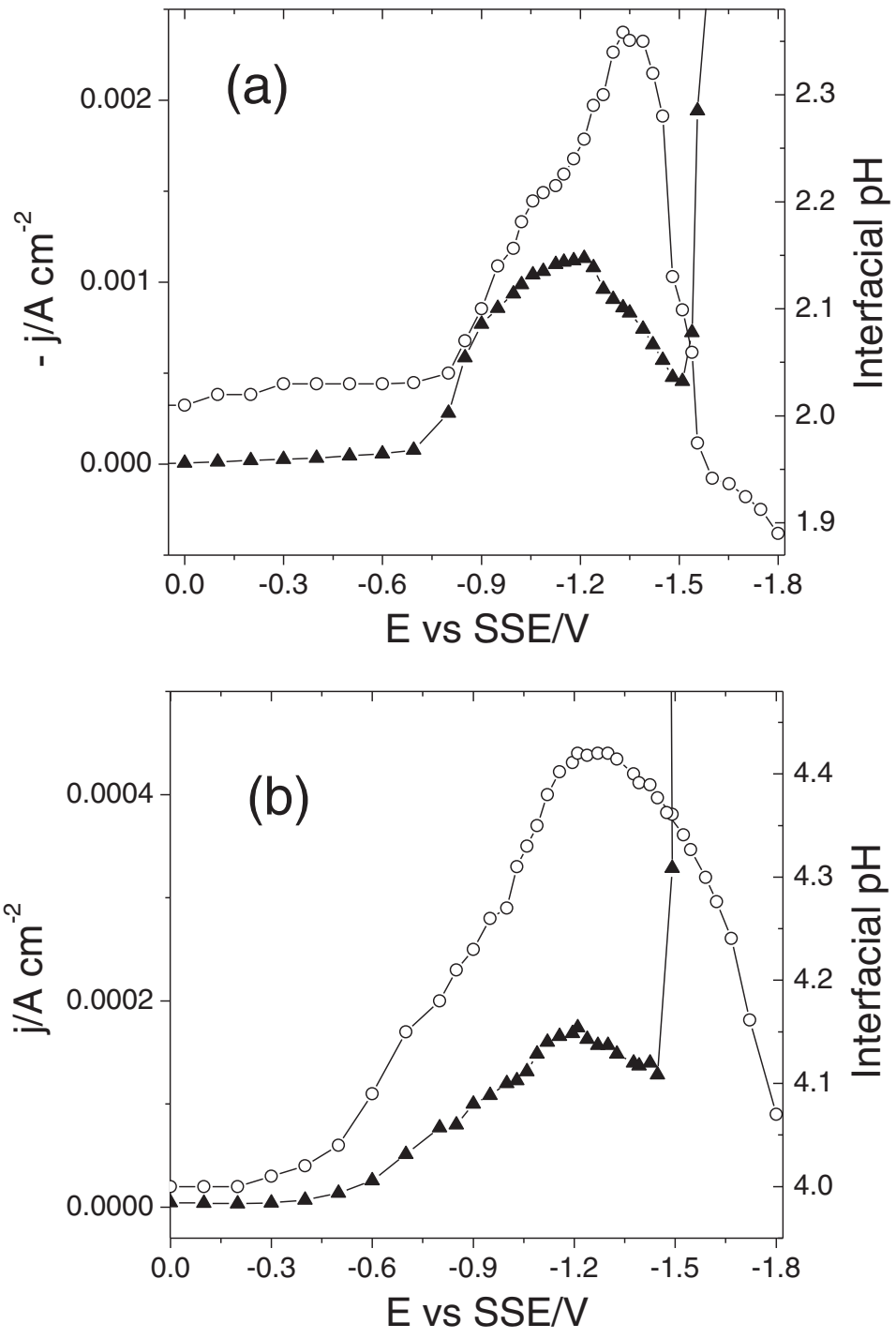

Fig. 3. Potential dependency of both interfacial pH (○) and current (▲) obtained simultaneously in the 1 M $ZnSO_4{\cdot}7H_2O$ solution at bulk pH values of: (a) 2 and (b) 4.

raise, which confers an abrupt change in the slope of the curves that start to vary sharply with cathodic potential (Part 2). High efficient Zn deposition was detected at this part of the curves for all the pH values investigated.

With increasing pH, a decrease in current densities at Part 1 of the curves is verified in Fig. 1. For each pH value, a current maximum is also detected in this potential range, which depends on the solution pH. Indeed, the current maximum is less intense and shifted to more negative potentials with higher pH, namely −1.20, −1.26, and −1.34 V for pH 2, 3, and 4, respectively. After the corresponding maximum, all curves present a decrease in current values before an abrupt increase with polarization. Moreover, Part 2 of the curves begins at more positive potentials and also positively shifted with increasing pH. Since high efficient Zn electrodeposition occurs in this region, this behaviour indicates an activation of this process with increasing pH. This result is in agreement with that reported by Epelboin et al. [1,2] for Zn electrodeposition from sulphate solutions.

Fig. 2 displays the comparative behaviour of cathodic polarization curves obtained in 1.0 M Na_2SO_4 (Zn^{2+}-free) and 1.0 M $ZnSO_4{\cdot}7H_2O$ solutions at pH 2.0, at the potential range corresponding to Part 1 of the curves in Fig. 1. It can be noted that, for the Zn^{2+}-free solution, the current increases continuously with cathodic potential. Moreover, for a given

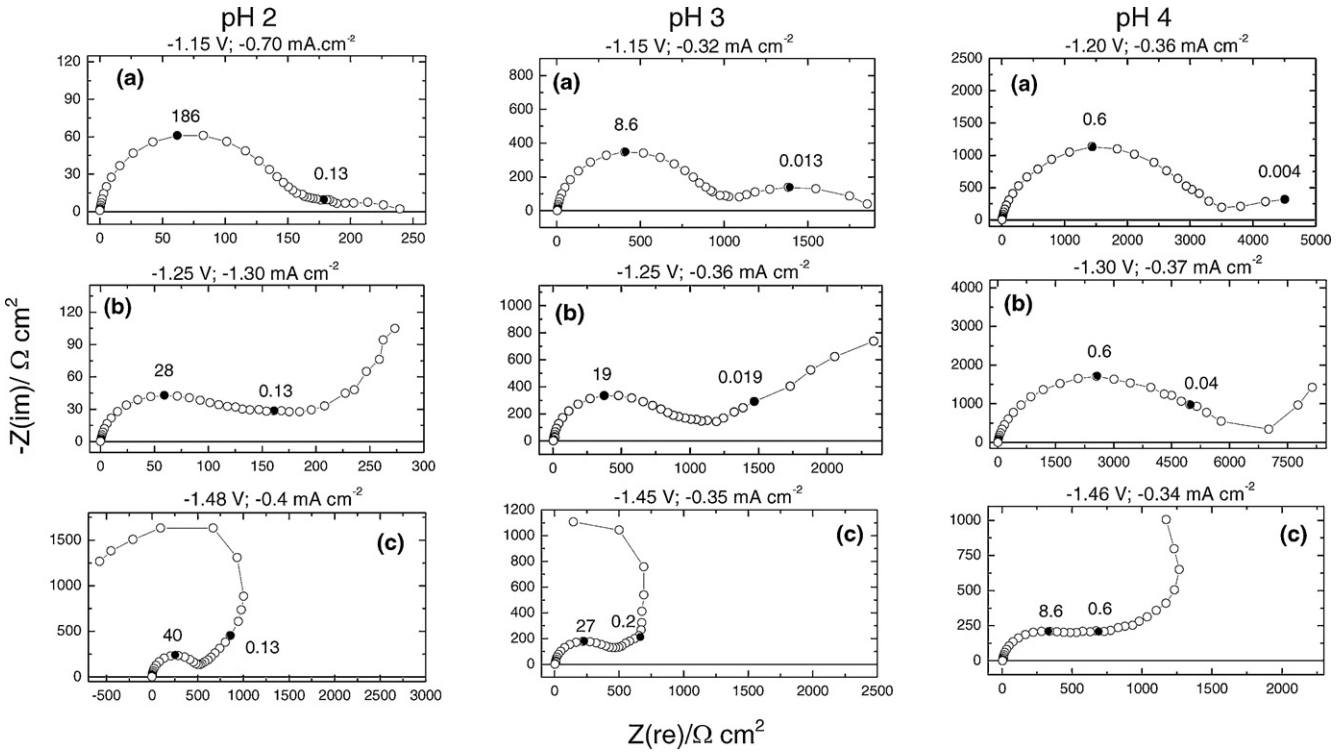

Fig. 4. Impedance diagrams obtained in the 1 M $ZnSO_4{\cdot}7H_2O$ solution at different pH values: (a) before; (b) during and (c) after the current maximum in the polarization curves of Fig. 1 (frequencies in Hz).

potential the current values are considerably higher and no maximum is observed for the Zn^{2+}-free. The same comparative behaviour was observed for all the pH values investigated.

Measurements of the interfacial pH can be used to obtain information regarding not only the electrodeposition process itself, but also the associated interfacial surface chemistry. In this way, Fig. 3 shows the typical potential dependency of both interfacial pH and current during Zn electrodeposition on a Pt surface from the solution at pH 2 and 4. For all the pH values investigated, a strong interface alkalination was observed before the current maximum at Part I of the curves. This corroborates the idea that hydrogen evolution prevails in this potential range. With increasing cathodic polarization, beyond the current maximum, both current and interfacial pH drop. At Part 2 of the curves, wherein high efficient Zn deposition occurs, a less accentuated decrease on the interfacial pH with increasing potential was verified for all the pH values investigated. No further alkalination was detected in this potential range. Moreover, no H_2 bubbles on the electrode surface were seen during Zn electrodeposition. This result is in disagreement with Van Parys et al. [12] that considered that Zn electrodeposition from acid sulphate solution occurs by means of a strong interface akalination.

Fig. 4 presents the impedance diagrams obtained in potentiostatic mode at the potential range corresponding to Part 1 of the polarization curves in Fig. 1. In all diagrams, the capacitive loop at higher frequencies is associated with the double layer response. For the three pH values investigated, the diagrams obtained before the current maxima, diagrams (a), display one capacitive loop in the low frequency domain, with corresponding characteristic frequencies (the frequency at the maximum) of 0.13, 0.013, and 0.006 Hz for pH 2, 3 and 4, respectively, in all cases related to the H^+ reduction. With increasing polarization, diagrams (b), at potential values associated with the current maxima in the curves of Fig. 1, a new capacitive loop appears at lower frequencies. The large size of this loop suggests the emergence of a surface competitive process between new adsorbed species and the H^+ reduction. After the current maxima, diagrams (c), the capacitive loop at lower frequencies shows a negative polarization resistance (R_p) for the three solution pH investigated. These results are in conformity with the decrease in current values, i.e., with the negative slope, namely polarization resistance, observed in Part 1 of the curves in Fig. 1.

Representative diagrams obtained in a Zn^{+2}-free solution (1 M Na_2SO_4) at pH 2 are shown in Fig. 5. These diagrams were acquired in potentiostatic mode at the same corresponding potential values as those for the 1 M $ZnSO_4{\cdot}7H_2O$ solution in the same pH value (Fig. 4). In Fig. 5(a), the diagram shows two capacitive loops (60 and 0.013 Hz) associated respectively with the double layer response and the H^+ reduction as the single cathodic reaction. The similarity between this diagram and the corresponding one in Fig. 4(a), pH 2, confirms that the H^+ reduction is the major cathodic reaction at this potential region for the 1 M $ZnSO_4{\cdot}7H_2O$ solution. With increasing potential, however, Fig. 5(b) and (c), the diagrams are qualitatively the same as the one obtained at lower potential in Fig. 5(a). They show two capacitive loops: 400 and 0.13 Hz at −1.20 V; and 1500 and 1.3 Hz for −1.40 V; also related respectively to the double layer response and the H^+ reduction process, Given that no competitive aspect is observed in the Zn^{2+}-free solution, Fig. 5, the results in Fig. 4 thus reflect the predominance of H^+ reduction reaction and a subsequently competitive effect brought about by an adsorbed intermediate for Zn electrodeposition.

Fig. 6 presents the impedance diagrams obtained in galvanostatic mode at Part 2 of the polarization curves in Fig. 1 for pH 2, 3 and 4 at three different potential values. For each diagram, the capacitive loop at high frequencies is related to the charge transfer resistance in parallel with the double layer capacitance. At the beginning of Part 2, Fig. 6(a–c), the diagrams depict two inductive loops in the low frequencies domain for all pH values investigated. This behaviour can be associated with Zn^{2+} reduction as the main cathodic reaction. With increasing polarization three inductive loops can be seen for pH 2, Fig. 6(d). At even higher polarization,

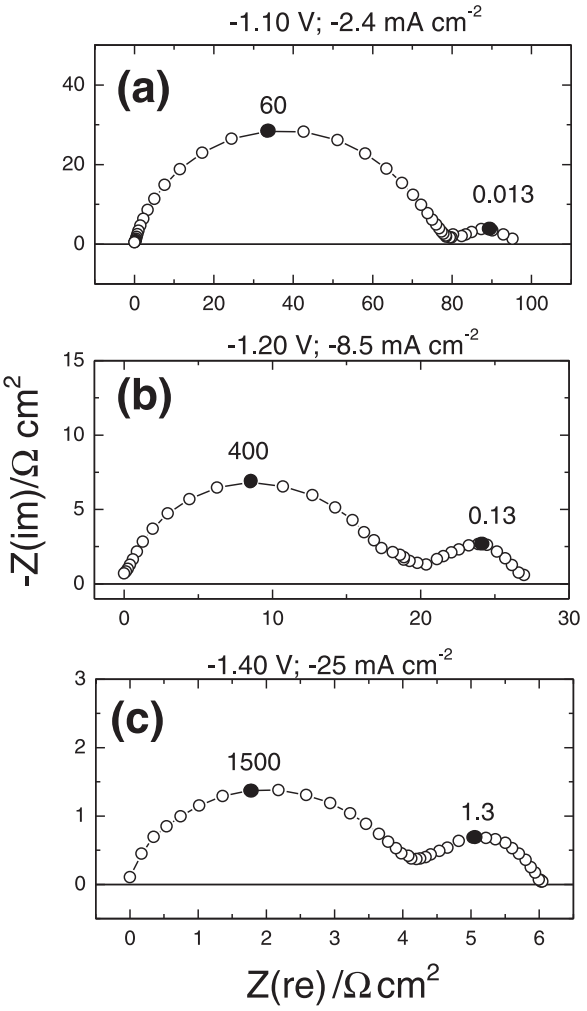

Fig. 5. Impedance diagrams obtained in the 1 M Na_2SO_4 (Zn^{2+}-free) solution, pH 2, at the corresponding potential values of diagrams obtained in 1 M $ZnSO_4{\cdot}7H_2O$, pH 2, in Fig. 4 (frequencies in Hz).

Fig. 6(g), the inductive loop at very low frequencies is replaced by a capacitive feature that cannot be described by the available models for Zn electrodeposition [1–8]. For pH 3, Fig. 6(e) and (h), the same tendency with increasing polarization is observed. However, this behaviour is slower as a function of the polarization, if compared to pH 2. Indeed, for pH 2 the capacitive loop is evident in −1.59 V, whereas, for the same polarization, this feature is not well defined in pH 3. Moreover, for pH 4, Fig. 6(f) and (i), the diagrams always exhibit three inductive loops. In view of the trend observed for the behaviour at pH 2–3, a capacitive loop would also be expected at higher polarizations.

Fig. 7 displays the cathodic polarization curves obtained with Zn RDE in 1 M $ZnSO_4{\cdot}7H_2O$ solution at pH values of 2, 3 and 4. Similar to Fig. 1, these curves can be divided in two regions as well. Starting at the open circuit potential, the curves present a very slow variation of current with cathodic polarization (Part 1). However, different from Fig. 1, where the curves were obtained with Pt RDE, no current maxima are observed in this potential range for the Zn RDE electrode (Fig. 7). In addition, no clear pH dependence is observed in Part 1 of these curves. With further polarization increase, the curves show the same qualitative behaviour as the corresponding ones obtained with the Pt RDE (Fig. 1), i.e., a sharp increase of current with cathodic potential (Part 2). The pH dependence of Part 2 of the curves in Fig. 7 is also analogous to that verified in Fig. 1, namely, the curves are shifted towards more positive potentials with increasing pH. The similarity on the behaviour of Part 2 of the curves for both Pt (Fig. 1) and Zn (Fig. 7) RDE suggests that, at the beginning of this potential range (current minimum), the Pt RDE is already covered by a metallic Zn film.

The impedance diagram obtained in galvanostatic mode with Zn RDE at the marked point (**p**), which corresponds to the beginning of Part 2 of the polarization curve for pH 2 in Fig. 7, exhibits two inductive loops in the low frequency domain. This diagram is comparable to the ones in Fig. 6(a–c), obtained with Pt RDE. This corroborates the idea of similar surface condition for both Pt and Zn RDE electrodes in 1 M $ZnSO_4{\cdot}7H_2O$ solution at beginning of Part 2 of the respective polarization curves.

4. Discussion

As presented above, independent of the solution pH, two distinct potential regions in the polarization curves of Fig. 1 were detected as a function of the cathodic potential. At low polarizations, Part 1, the efficiency for Zn deposition is very low and the main cathodic reaction is the H^+ reduction on a Pt surface. Only at the end of Part 1, where the current reaches a minimum, the main cathodic reaction becomes the Zn^{2+} reduction. Under this condition, the Pt surface becomes covered by a metallic Zn film. Subsequently, Zn deposition occurs with high efficiency on a Zn surface all through the Part 2 of the curves. For simplification and to make easier the discussion, a reaction model for Zn electrodeposition in acid sulphate solution on a Pt RDE is proposed as divided into two parts, considering the two above-mentioned potential regions.

4.1. Part 1

Some aspects related to this potentials region are emphasized below:

I. Regardless the solution pH, the current maximum at Part 1 of the polarization curves comes up as a consequence of a competition between the hydrogen reduction reaction, which prevails in this potential range, and surface reactions with the participation of Zn^{2+} ions. The absence of current maxima in the polarization curves obtained in the Zn^{2+}-free solution corroborates such behaviour.
II. In Part 1, there is a current maximum that depends on the pH of the solution. With increasing pH, the current value associated with this maximum decreases and is shifted to more negative potentials.
III. Apart from the bulk solution pH, the interfacial pH increases up to the current maximum and then starts to decrease. Consequently, the reaction process responsible for the current decreasing also accounts for the interfacial pH drop up to the current minimum.
IV. Impedance diagrams taken at the potential range corresponding to Part 1 of the polarization curves display, besides the capacitive loop related to the double layer response, up to two time constants associated with the formation of two adsorbed intermediates at the electrode surface.

To account for these features, the following reaction model can be considered for Part 1 of the polarization curves in Fig. 1:

$$H^+ + e^- \xrightarrow{K_{-1}} H_{ads} \quad (\theta_1 \equiv H_{ads}) \tag{1}$$

$$H^+ + H_{ads} + e^- \xrightarrow{K_{-2}} H_2 \tag{2}$$

$$Zn^{2+} + H_{ads} + H^+ + 2e^- \underset{K_3}{\overset{K_{-3}}{\rightleftarrows}} [Zn(I) - H]^+_{ads} + H \quad (\theta_2 \equiv [Zn(I) - H]^+_{ads}) \tag{3}$$

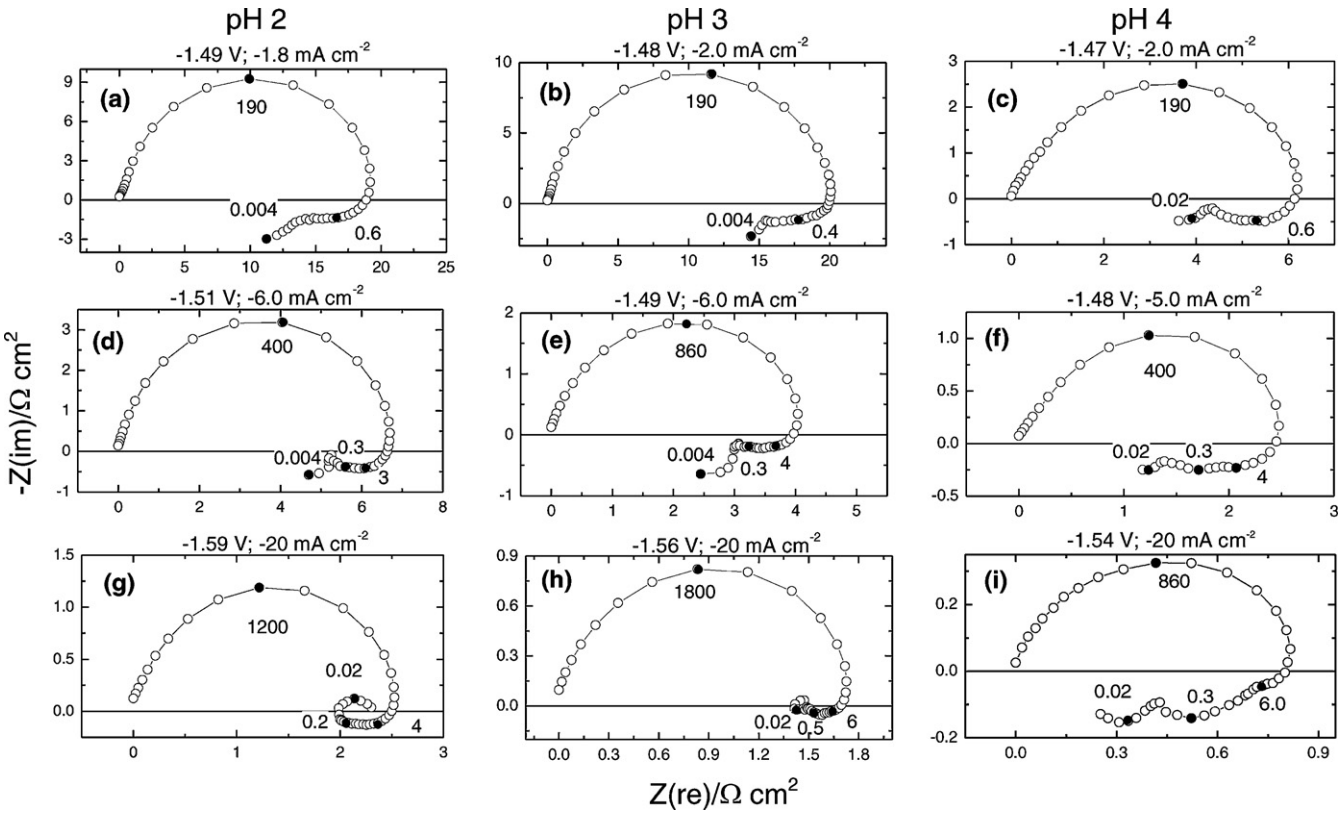

Fig. 6. Impedance diagrams obtained in the 1 M $ZnSO_4{\cdot}7H_2O$ solution at different pH values at the indicated potential/current density values (frequencies in Hz).

$$[Zn(I)-H]^{+}_{ads} \xrightarrow{K_q} Zn + H^{+} \quad (4)$$

$$Zn^{2+} + [Zn(I)-H]^{+}_{ads} + OH^{-} + 2e^{-} \xrightarrow{K_{-4}} 2Zn + H_2O \quad (5)$$

where θ_i corresponds to the electrode coverage by the corresponding adsorbed specie *i*.

Reactions (1) and (2) reflect the H^+ reduction with further hydrogen evolution on the Pt surface. These steps give an explanation for the surface alkalination at Part 1 of the curves before the current maximum, wherein the hydrogen reduction prevails, as shown in Fig. 3.

With increasing polarization, reaction (3) in the forward direction becomes significant and, consequently, the $[Zn(I)-H]^{+}_{ads}$ intermediate starts to replace H_{ads} at the electrode surface. Indeed, from this reaction, the formation of $[Zn(I)-H]^{+}_{ads}$ occurs at the expenses of H_{ads}. Since in this potential region the efficiency for Zn deposition is very low, the rate of reaction (4) is considered to be not negligible. This means that the enhancement of θ_2 does not compensate the vanishing of θ_1 in terms of current contribution. As a result, the current starts to decrease with the establishing of a maximum. The origin of this current maximum is hence a function of the θ_2/θ_1 ratio, as will be further discussed in this work.

As a consequence of reaction (3) in the forward direction, chemical reaction (4) starts to occur with the decomposition of $[Zn(I)-H]^{+}_{ads}$ and the formation of H^+. This is the reaction that causes the pH decrease from the maximum up to the current minimum (Fig. 3). At this point, reaction (5) prevails, being responsible for the coverage of the entire surface by metallic Zn.

Given the above discussion and considering that the Langmuir isotherm law is valid, wherein θ_i is a potential and time dependent parameter, the current associated with the above set of reactions can be described by the following equation:

$$\frac{I}{F} = -K_{-1}[H^+](1-\theta_1-\theta_2) - K_{-2}[H^+]\theta_1 - 2K_{-3}[H^+]\theta_1 + 2K_3\theta_2 - 2K_{-4}[OH^-]\theta_2 \quad (6)$$

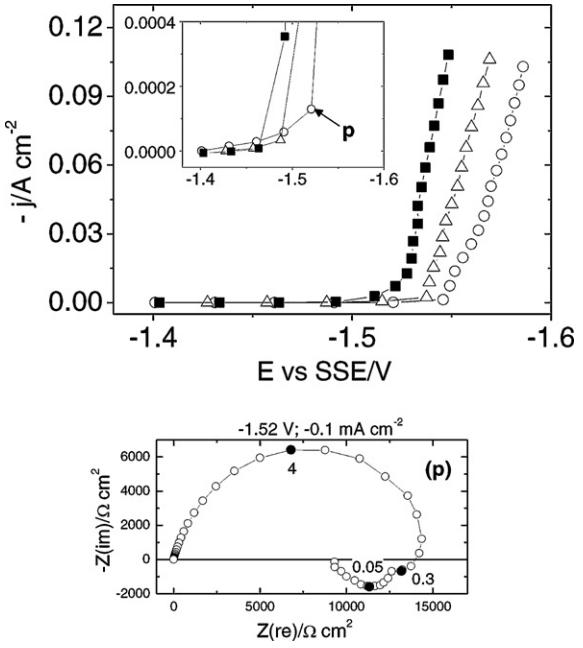

Fig. 7. Steady state cathodic polarization curves of Zn RDE in the 1 M $ZnSO_4{\cdot}7H_2O$ solution at pH 2 (○), 3 (△), 4 (■) and impedance diagram obtained at marked point (p) (frequencies in Hz).

The mass balance leads to:

$$\beta\frac{d\theta_1}{dt} = K_{-1}[H^+](1-\theta_1-\theta_2) - K_{-2}[H^+]\theta_1 - K_{-3}[H^+]\theta_1 + K_3\theta_2 \quad (7)$$

$$\beta\frac{d\theta_2}{dt} = K_{-3}[H^+]\theta_1 - K_3\theta_2 - K_{-4}[OH^-]\theta_2 - K_q\theta_2 \quad (8)$$

At the steady state, $\beta d\theta_1/dt = 0$ and $\beta d\theta_2/dt = 0$. Then,

$$-K_{-1}[H^+](1-\theta_1-\theta_2) = -K_{-2}[H^+]\theta_1 - K_{-3}[H^+]\theta_1 + K_3\theta_2 \quad (9)$$

and

$$-K_{-3}[H^+]\theta_1 + K_3\theta_2 = -K_{-4}[OH^-]\theta_2 - K_q\theta_2 \quad (10)$$

Replacing Eq. (10) in Eq. (9) results in:

$$-K_{-1}[H^+](1-\theta_1-\theta_2) = -K_{-2}[H^+]\theta_1 - K_{-4}[OH^-]\theta_2 - K_q\theta_2 \quad (11)$$

By applying Eqs. (10) and (11) in Eq. (6), the expression for the steady state current becomes:

$$\frac{I}{F} = -2K_{-2}[H^+]\theta_1 - 5K_{-4}[OH^-]\theta_2 - 3K_q\theta_2 \quad (12)$$

Since $\theta_1 >> \theta_2$ at the beginning of the polarization curves, from the open circuit potential up to the current maximum, the only contribution to the current is given by the term $-2K_{-2}[H^+]\theta_1$, that is, by the H^+ reduction. From this term, the higher the pH the lower is the current, as observed from the experimental results (Fig. 1).

From the current maximum, wherein θ_2 appears, the current turns out to be equivalent to $-2K_{-2}[H^+]\theta_1 - 5K_{-4}[OH^-]\theta_2 - 3K_q\theta_2$. This expression comprises the current drop after the current maximum, also verified in Fig. 1. According to this expression, the current diminishes with further potential increase since $-5K_{-4}[OH^-]\theta_2 - 3K_q\theta_2$ is not able to balance the decrease on the term $-2K_{-2}[H^+]\theta_1$. When the current minimum is attained, where $\theta_2 \gg \theta_1$, the current then corresponds to $-5K_{-4}[OH^-]\theta_2 - 3K_q\theta_2$. In this condition, it is clear that the polarization corresponding to the minimum would be lower at higher pH. This fact accounts for the positive shift of the current minimum experimentally observed (Fig. 1).

As previously discussed, the potential corresponding to the current maximum observed at Part 1 of the polarization curves (Fig. 1) is established by the θ_2/θ_1 ratio. From Eq. (10), it follows that

$$\frac{\theta_2}{\theta_1} = \frac{K_{-3}[H^+]}{K_3 + K_{-4}[OH^-] + K_q}$$

However, since in the current maximum $K_{-4}[OH^-]$ is very small, the above expression reduces to:

$$\frac{\theta_2}{\theta_1} = \frac{K_{-3}[H^+]}{K_3 + K_q}$$

Taking this expression into account, a higher pH causes a decreasing in the θ_2/θ_1 ratio. This means that a higher polarization would be required for a proper θ_2/θ_1 ratio to occur, giving rise to the current maximum. This fact justifies the shift of current maximum towards more negative potentials with increasing pH, as seen in Fig. 1.

From Eq. (6) the faradaic impedance, Z_F, can be obtained:

$$\frac{1}{Z_F} = \frac{1}{R_t} - F\left\{-K_{-1}[H^+] + K_{-2}[H^+] + 2K_{-3}[H^+]\right\}\frac{\tilde{\theta}_1}{\tilde{E}} - F\left\{-K_{-1}[H^+] - K_3 + 2K_{-4}[OH^-]\right\}\frac{\tilde{\theta}_2}{\tilde{E}} \quad (13)$$

where R_t is the charge transfer resistance, F is the Faraday's constant, $\tilde{\theta}_1/\tilde{E}$ and $\tilde{\theta}_2/\tilde{E}$ represent the respective surface concentration relaxations of H_{ads} and $[Zn(I)-H]^+_{ads}$ resulting from the sine perturbation of the cathodic potential.

Before the current maximum, regardless of pH, the impedance diagrams, Fig. 4(a), show the presence of a capacitive loop at low frequencies related to the H^+ reduction. From the present reaction model, the $\tilde{\theta}_1/\tilde{E}$ relaxation in Eq. (13) will give rise to a capacitive loop if:

$$-K_{-1}[H^+] + K_{-2}[H^+] + 2K_{-3}[H^+] > 0$$

That can also be written as

$$K_{-2}[H^+] + 2K_{-3}[H^+] > K_{-1}[H^+] \quad (14)$$

The condition given by Eq. (14) is in accordance with the reaction model proposed for Part 1, once that, at low potentials, the current is mainly related to K_{-2}. Eq. (14) should be valid for larger polarizations as well, since the capacitive loop associated with the $\tilde{\theta}_1/\tilde{E}$ relaxation is present in the diagrams, Fig. 4(b) and (c). Indeed, Eq. (14) is also valid after the current maximum up to the minimum in Part 1 of the polarization curves, in view of the fact that K_{-3} prevails in such conditions.The analysis of the capacitive loop at lower frequencies should comprise the negative polarization resistance (R_p), verified in Fig. 4(c), in association with $\tilde{\theta}_2/\tilde{E}$ relaxation. To justify this behaviour, a very precise mathematical condition must be established [18–20]. Moreover, the presence of $R_p < 0$ in the diagrams of Fig. 4(c) is in agreement with the current drop due to θ_2, as proposed by the present model for Part 1.

4.2. Part 2

As mentioned before, starting at the current minimum, the electrode surface is already covered by metallic Zn. Under this condition, the adsorbed species previously formed onto the Pt surface no longer exists and new intermediates would be formed. This implies that the reaction mechanism for Part 2 of the curves must be distinct from that for Part 1. In fact, the reaction model proposed to Part 1 gives rise to a metallic Zn surface onto the Pt electrode at the current minimum. Some relevant aspects related to Part 2 of the curves can be stressed as follows:

I. Starting at the current minimum, the current varies sharply with cathodic potential. This current minimum, and consequently Part 2 of the curves, occurs at more positive potentials for higher pH values. Moreover, for a given potential in this region, the current increases with increasing pH.
II. For the three pH values investigated, at the very beginning of Part 2 of the polarization curves the impedance diagrams show only two inductive loops, in addition to the capacitive loop related to the double layer relaxation. With increasing polarization a third inductive loop appears in the low frequency range. This loop turns into capacitive with further polarization increase, being this phenomenon highly pH dependent. In fact, this capacitive loop at high polarizations becomes harder to observe the higher is the pH.
III. The variation of interfacial pH during Zn electrodeposition in Part 2 is smaller than in Part 1 (Fig. 3). Therefore, the H^+ consumption at the electrode surface is not as important as in Part 1.

According to these facts, the following reaction model is proposed to Part 2 of the polarization curves:

$$Zn^{2+} + H_2O + e^- \underset{K_1}{\overset{K_{-1}}{\rightleftarrows}} [Zn(I)-H_2O]^+_{ads} \quad (\theta_3 \equiv [Zn(I)-H_2O]^+_{ads}) \quad (15)$$

$$Zn^{2+} + [Zn(I)-H_2O]^+_{ads} + 2e^- \xrightarrow{K_{-2}} [Zn(I)-H_2O]^+_{ads} + Zn \quad (16)$$

$$Zn^{2+} + [Zn(I) - H_2O]^+_{ads} + SO_4^{2-} + 2e^- \overset{K_{-3}}{\underset{K_3}{\rightleftarrows}} [Zn(I) - OH]^+_{ads} + Zn + HSO_2^- \quad (\theta_4 \equiv [Zn(I) - OH]^+_{ads}) \tag{17}$$

$$Zn^{2+} + [Zn(I) - OH]^+_{ads} + 2e^- \xrightarrow{K_{-4}} [Zn(I) - OH]^+_{ads} + Zn \tag{18}$$

$$H^+ + [Zn(I) - OH]^+_{ads} + e^- \xrightarrow{K_{-5}} H_{ads} + [Zn(I) - OH]^+_{ads} \quad (\theta_5 \equiv H_{ads}) \tag{19}$$

$$H^+ + H_{ads} + e^- \xrightarrow{K_{-6}} H_2 \tag{20}$$

where θ_i corresponds to the electrode coverage by the corresponding adsorbed specie *i*.

Reaction (15) shows the formation of the initial adsorbed intermediate $[Zn(I) - H_2O]^+_{ads}$ on a Zn surface. Subsequently, this intermediate participates in the formation of metallic Zn through the autocatalytic reaction (16). The $[Zn(I) - H_2O]^+_{ads}$ also produces the $[Zn(I) - OH]^+_{ads}$ species via reaction (17), which participates in an autocatalytic reduction of Zn^{2+} to metallic Zn in reaction (18). The two inductive loops in the low frequency range exhibited in Fig. 6(a)–(c) and 7(p) are related to the relaxation of these species.

Reactions (15)–(18) are primarily responsible for the current rise in Part 2 and accounts for the higher currents verified with increasing pH in this potential region. According to the equilibrium $HSO_4^- \leftrightarrow H^+ + SO_4^{2-}$, the higher the pH, the higher is the sulphate concentration. Thus, the higher the pH, the greater $[Zn(I) - OH]^+_{ads}$ and, as a consequence, the faster reaction (18) will be.

The formation of H_{ads} is responsible for the emergence of the inductive loop at lower frequencies. This intermediate is produced via step (19) and is catalyzed by the species $[Zn(I) - OH]^+_{ads}$. Hence, the higher the surface concentration of this species, the lower the cathodic polarization for the H_{ads} formation will be, with the consequent appearance of the third inductive loop, as shown in Fig. 6.

The rate of reaction (20) decreases with increasing pH. Therefore, the higher the pH, the larger the cathodic polarization in which K_{-6} becomes higher than K_{-5}. Under this condition, the inductive loop at lower frequency turns into a capacitive one, as will be discussed later.

Considering that the Langmuir isotherm is valid and that θ_i is a potential and time dependent parameter, the current and mass balance associated with the set of reactions (15)–(20) are given by:

$$\frac{I}{F} = -K_{-1}(1 - \theta_3 - \theta_4 - \theta_5) + K_1\theta_3 - 2K_{-2}\theta_3 - 2K_{-3}[SO_4^{2-}]\theta_3 + 2K_3[HSO_4^-]\theta_4 - 2K_{-4}\theta_4 - K_{-5}[H^+]\theta_4 - K_{-6}[H^+]\theta_5 \tag{21}$$

and

$$\beta\frac{d\theta_3}{dt} = K_{-1}(1 - \theta_3 - \theta_4 - \theta_5) - K_1\theta_3 - K_{-3}[SO_4^{2-}]\theta_3 + K_3[HSO_4^-]\theta_4 \tag{22}$$

$$\beta\frac{d\theta_4}{dt} = K_{-3}[SO_4^{2-}]\theta_3 - K_3[HSO_4^-]\theta_4 \tag{23}$$

$$\beta\frac{d\theta_5}{dt} = K_{-5}[H^+]\theta_4 - K_{-6}[H^+]\theta_5 \tag{24}$$

At the steady state, $\beta\frac{d\theta_3}{dt} = \beta\frac{d\theta_4}{dt} = \beta\frac{d\theta_5}{dt} = 0$, then Eqs. (22)–(24) can be written as

$$K_{-1}(1 - \theta_3 - \theta_4 - \theta_5) - K_1\theta_3 = K_{-3}[SO_4^{2-}]\theta_3 - K_3[HSO_4^-]\theta_4 \tag{25}$$

$$K_{-3}[SO_4^{2-}]\theta_3 - K_3[HSO_4^-]\theta_4 = 0 \tag{26}$$

$$K_{-5}[H^+]\theta_4 - K_{-6}[H^+]\theta_5 = 0 \tag{27}$$

By applying Eq. (25) in Eq. (26), it follows

$$K_{-1}(1 - \theta_3 - \theta_4 - \theta_5) - K_1\theta_3 = 0 \tag{28}$$

Eqs. (26) and (28) show that, at the steady state, the reactions (15) and (17) are in equilibrium. By applying Eqs. (26)–(28) in Eq. (21), the stationary current is given by:

$$\frac{I}{F} = -2K_{-2}\theta_3 - 2K_{-4}\theta_4 - 2K_{-6}[H^+]\theta_5 \tag{29}$$

According to the interfacial pH measurements that show a small variation in Part 2 (Fig. 3) irrespective of the bulk pH, θ_5 will always be smaller if compared with θ_3 and θ_4. Therefore, regardless of the bulk pH, the partial current term $-2K_{-6}[H^+]\theta_5$ will always be smaller if compared with $-2K_{-2}\theta_3 - 2K_{-4}\theta_4$. Thus, the current given by Eq. (29) is mainly associated with the first two terms. In this way, the current increases with increasing pH since, according to reactions (15) and (17), θ_3 and θ_4 increase with increasing pH. This is in conformity with the experimental data in Figs. 1 and 7 related to Part 2 of the polarization curves.

From Eq. (21), the expression for the faradaic impedance, Z_F, is given by:

$$\frac{1}{Z_F} = \frac{1}{R_t} - F\left\{-K_{-1} - K_1 + K_{-2} + 2K_{-3}[SO_4^{2-}]\right\}\frac{\tilde{\theta}_3}{\tilde{E}} - F\left\{-K_{-1} - 2K_3[HSO_4^-] + 2K_{-4} + K_{-5}\right\}\frac{\tilde{\theta}_4}{\tilde{E}} - F\left\{-K_{-1} + K_6[H^+]\right\}\frac{\tilde{\theta}_5}{\tilde{E}} \tag{30}$$

where R_t is the charge transfer resistance and $\tilde{\theta}_3/\tilde{E}$, $\tilde{\theta}_4/\tilde{E}$, and $\tilde{\theta}_5/\tilde{E}$ are the respective relaxations of surface concentrations of the intermediates $[Zn(I) - H_2O]^+_{ads}$, $[Zn(I) - OH]^+_{ads}$ and H_{ads}, resulting from the sine perturbation of the cathodic potential.

To justify the experimental electrochemical impedance results shown in Fig. 6, the relaxation of both $\tilde{\theta}_3/\tilde{E}$ and $\tilde{\theta}_4/\tilde{E}$ should provide inductive loops in the whole polarization range investigated. On the other hand, $\tilde{\theta}_5/\tilde{E}$ relaxation should originate an inductive loop, which turns into capacitive at high polarizations. In view of Eq (30), to oblige this to occur, the following assumptions are required:for $\tilde{\theta}_3/\tilde{E}$

$$-K_{-1} - K_1 + K_{-2} + 2K_{-3}[SO_4^{2-}] < 0 \text{ or } K_{-1} + K_1 > K_{-2} + 2K_{-3}[SO_4^{2-}] \tag{31}$$

for $\tilde{\theta}_4/\tilde{E}$

$$-K_1 - 2K_3[HSO_4^-] + 2K_{-4} + K_{-5} < 0 \text{ or } K_{-1} + 2K_3[HSO_4^-] > 2K_{-4} + K_{-5} \tag{32}$$

for $\tilde{\theta}_5/\tilde{E}$

$$-K_{-1} + K_6[H^+] < 0 \text{ or } K_6[H^+] < K_{-1} \tag{33}$$

Reaction (15) in the forward direction (K_{-1}) produces $[Zn(I) - H_2O]^+_{ads}$, which gives rise to two other intermediates, $[Zn(I) - OH]^+_{ads}$ and H_{ads}. To satisfy this condition, K_{-1} has to be higher than K_{-3} over the entire potential range. This fact confirms that the assumption of Eq (31) is in agreement with the proposed model for Part 2.

The value of K_{-5} is not high enough during the whole polarization range associated with Part 2 since, according to Fig. 3, the variation of the interfacial pH is small in this region. Moreover, taking into account that K_{-4} is the rate of the autocatalytic step (18) for Zn metallic formation, it is reasonable to consider that, based on the proposed model for Part 2, the condition imposed by Eq. (32) is valid over this entire potential range.

The condition in Eq. (33) involves the term $-K_{-1} + K_6[H^+]$, whose signal depends on the polarization. At the beginning of Part 2, this term is negative, given that $K_6[H^+] < K_{-1}$. In this case, the relaxation

$\tilde{\theta}_5/\tilde{E}$ will originate an inductive loop. With increasing cathodic polarization, K_{-6} increases progressively in such a way that, at a particular potential, $K_6[H^+] > K_{-1} > 0$. In this circumstance, the $\tilde{\theta}_5/\tilde{E}$ relaxation generates a capacitive loop. Thus, the conversion of the inductive loop at lower frequencies into a capacitive one, as seen in Fig. 6, is associated with the changing of $K_6[H^+] < K_{-1}$ to $K_6[H^+] > K_{-1}$. Taking into account that the H^+ concentration favours the condition $K_6[H^+] > K_{-1}$, the higher the pH, the higher should be the cathodic polarization for this transformation to occur, as discussed earlier in this article and verified in the experimental plots in Fig. 6.

5. Conclusions

The polarization curves of a Pt RDE in Zn sulphate acid solutions at pH values of 2, 3, and 4 show two distinct regions. Part 1 reflects mainly the H^+ reduction on a Pt surface, and in Part 2, where the current varies sharply with the potential, the major cathodic reaction is Zn electrodeposition on a Zn surface.

Part 1 of the polarization curves display a current maximum and a current minimum, regardless the solution pH. From the open circuit potential up to the current maximum, the interfacial pH increases and then decreases until the current minimum is attained. With increasing solution pH, the current associated with this maximum decreases and is shifted to more negative potentials. Conversely, the current minimum, and thus Part 2 of the curves, occurs at more positive potentials for higher pH values. Moreover, for a given potential at Part 2, the current increases with increasing pH.

The kinetics at Part 1 comprises two adsorbed intermediates onto the Pt surface. One of them is responsible for the hydrogen evolution and the other species is associated with the Zn^{2+} reduction. The competition between the reactions that involve these two intermediates originates not only a current decrease up to the minimum but also the interfacial pH drop as well as the negative polarization resistance in the impedance diagrams. The relative predominance of these species justifies the pH dependence of Part 1 of the curves.

Three adsorbed intermediates onto a metallic Zn surface exist at Part 2 of the polarization curves. These species are distinct from those at Part 1, which are adsorbed on the Pt surface.

The proposed reaction model indicates that the relative rate of formation and the surface concentration of the different intermediates depend on the solution pH, electrode potential and surface nature.

Acknowledgements

The authors are grateful to the support given by the Brazilian agencies: CNPq, FAPERJ, CAPES, FINEP and FUJB.

References

[1] I. Epelboin, M. Ksouri, R. Wiart, J. Electrochem. Soc. 122 (1975) 1206.
[2] I. Epelboin, M. Ksouri, E. Lejay, R. Wiart, Electrochim. Acta 20 (1975) 603.
[3] I. Epelboin, M. Ksouri, R. Wiart, Faraday Disc. Chem. Soc. 12 (1978) 115.
[4] J. Bressan, R. Wiart, J. Appl. Electrochem. 9 (1979) 615.
[5] I. Zouari, F. Lapique, Electrochim. Acta 37 (1992) 439.
[6] C. Cachet, R. Wiart, J. Appl. Electrochem. 20 (1990) 1009.
[7] C. Cachet, R. Wiart, J. Electrochem. Soc. 141 (1994) 131.
[8] R. Ichino, C. Cachet, R. Wiart, Electrochim. Acta 41 (1996) 1031.
[9] F. Ganne, C. Cachet, G. Maurin, R. Wiart, E. Chauveau, J. Petitjean, J. Appl. Electrochem. 30 (2000) 665.
[10] S.L. Díaz, O.R. Mattos, O.E. Barcia, F.J.F. Miranda, Electrochim. Acta 47 (2002) 4091.
[11] A. Gomes, M.I.S. Pereira, Electrochim. Acta 52 (2006) 863.
[12] H. Van Parys, G. Telias, V. Nadashkivskyi, B. Mollay, I. Vandendael, S. Van Damme, J. Deconinck, A. Hubin, Electrochim. Acta 55 (2010) 5709.
[13] K. Raeissi, A. Saatchi, M.A. Golozar, J.A. Szpunar, J. Appl. Electrochem. 34 (2004) 1249.
[14] D. Vasilakopoulos, M. Bouroushian, N. Spyrellis, Electrochim. Acta 54 (2009) 2509.
[15] T. Boiadjieva, M. Monev, A. Tomandl, H. Kronberger, G. Fafilek, J. Solid Electrochem. 13 (2009) 671.
[16] H. Deligianni, L.T. Romankiw, IBM J. Res. Dev. 37 (1993) 85.
[17] C. Deslouis, I. Frateur, G. Maurin, B. Tribollet, J. Appl. Electrochem. 27 (1997) 482.
[18] I. Epelboin, M. Keddam, O.R. Mattos, H. Takenouti, Proc. 7th International Congress of Metallic Corrosion, Rio de Janeiro, Brazil, 1979.
[19] M. Keddam, O.R. Mattos, H. Takenouti, Electrochim. Acta 31 (1986) 1147.
[20] M. Keddam, O.R. Mattos, H. Takenouti, Electrochim. Acta 31 (1986) 1159.